

Texas A&M Maroon Moon: Preliminary Surface Stabilization to Mitigate Lunar Plume Surface Interaction

Student Team

Travis Allen, Nathan Hung, Noah Kentros, Gautam Logeishwaran,
Jacob Milliken, and Andre Samaraweera

*Undergraduate Students, Department of Aerospace Engineering
Texas A&M University, College Station, TX, 77843*

Tehseena Ali

*Doctoral Student, Department of Civil Engineering
Texas A&M University, College Station, TX, 77843*

Faculty Advisors

John Connolly, PE

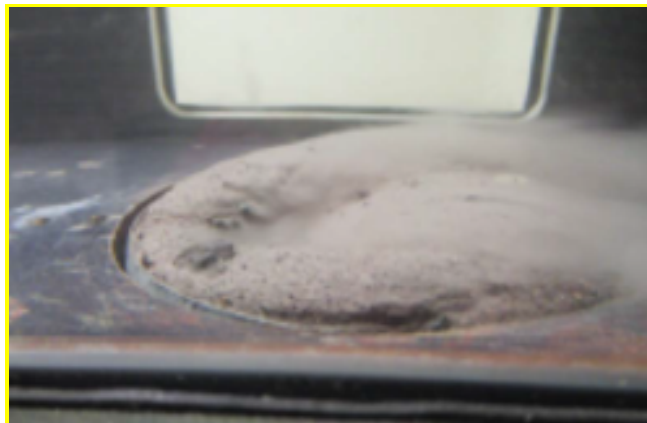
*Professor of Practice, Department of Aerospace Engineering
Texas A&M University, College Station, TX, 77843*



Jean-Louis Briaud, PhD, PE, Dist.M. ASCE

ASCE President 2021

*Distinguished Professor and Buchanan Chair Holder
Zachry Dpt. of Civil and Environmental Engineering
Texas A&M University, College Station, TX, 77843*



Texas A&M University Maroon Moon Team
Preliminary Surface Stabilization to Mitigate Plume-Surface Interaction

Major Objectives & Technical Approach

- Experiment with different soil sealants that prevent erosion of lunar regolith simulant
- Experiment was performed with water tunnel erosion device (EFA)
- Analytically compared water and air mediums by using boundary layer thickness ratios
- Preliminary design of two Gas-Granular Flow Apparatus (GGEA) flow tunnels to specifically model PSI through the measurement of erosion in a high velocity gas flow

Key Design Details & Innovations of the Concept

- Applying geotechnical erosion prevention techniques used on Earth to the lunar environment
- Using erosion function apparatus (EFA) to model PSI effects on lunar simulant
- Developing two unique gas-granular erosion apparatus (GGEA) that is designed to use high velocity exhaust gasses to accurately model PSI through erosion mechanisms

Image/Graphic:



Summary of Schedule & Costs for the proposed solution's path to adoption

- 2 year Development period
- Testing sealant solutions with EFA and beginning construction on the GGEA
- Validating Transformations between air and water mediums
- 2 year Operation period
- Testing chosen sealant solutions in the GGEA
- Construction of the CLPS Rover
- Testing rover application in a vacuum chamber
- Costs are from NASA Cost Estimation Toolkit (CET)
 - 2024: \$981,000, 2025: \$1,009,000, 2026: \$2,373,000, 2027: \$3,095,000

Table of Contents

I. Problem Statement and Report Outline	1
II. EFA Testing	1
A. Solution Choices	1
B. Materials and Methods	2
C. Results	3
III. CFD Analysis and GGEA Design	5
A. Analytical Water-to-Air Transformation	5
B. Gas-Granular Erosion Apparatus Design	11
IV. Discussion	13
A. EFA Assumptions and Errors	13
B. Solution Application on Lunar Surface	14
V. Further Implementation	15
A. Realistic Schedule and Milestones	15
B. Full Mission Timeline	15

I. Problem Statement and Background

Lunar plume surface interaction (PSI) is a phenomenon that can locally impact landing sites, causing damage to infrastructure in the area and the lander itself. The Maroon Moon team is approaching the problem of PSI as a form of high-speed erosion caused by exhaust gasses. To solve the problem, the team is focusing on solutions that modify the lunar landing site surface to stop exhaust gasses from diffusing into the pores of the lunar regolith. Because no specialized wind tunnel is available for testing, these solutions are first tested in a water tunnel using the Erosion Function Apparatus (EFA). Additionally, the team has designed plans for a Gas-Granular Erosion Apparatus (GGEA), a specialized wind tunnel that will model PSI and verify solutions from the EFA. To help facilitate the transition between the two mediums of water and air, an analytical transformation has been derived by comparing the boundary layer thicknesses.

II. EFA Testing

The erosion function apparatus (EFA) is a water based channel that is used to record and measure the erodibility of soils. The team has used an analogous relationship between Earth and Moon to test lunar soil in a water tunnel designed for Earth soils. The machine works by attaching a 76.2 mm diameter Shelby tube through the bottom of the channel where water flows at a given velocity. The lunar soil is then mechanically pushed by a piston out of the Shelby tube at a rate to match the erosion of the sample. By doing this, the displacement of the soil can be measured and the erosion rate can be calculated from the displacement over the time. The velocity of the water is measured by a flow sensor.

A. Solution Choices

In order to increase the cohesion of the lunar simulant JSC-1, the team analyzed tackifiers (Table 1), which are compounds that bind soil together. Tackifiers is an umbrella term with many compounds underneath such as polyacrylamide, guar, chloride compounds, resins, and various polymers. However most of these tackifiers were manufactured to be used on Earth where water is an abundant resource. For example the chloride compounds are required to be mixed with gallons of water and then sprayed on the soil to bind it together. This method of application cannot be used on the lunar surface, leading to this solution choice not being viable. Furthermore those organic tackifiers such as guar and resins are designed to withstand low speed wind forces not engine exhaust forces. The solution type that yielded the strongest force combined with the easiest application method was the polymer solutions, but that is still a broad category. To narrow down the specific solutions to test a trade study that analyzed pros, cons, cure time, and cost was made as shown below. From the tradestudy, light and medium cyanoacrylate glue was chosen as well as PLA plastic. All of these solutions offer a strong protection against erosion, have better UV protection than thermosets, and are mass efficient.

Table 1 Solutions tradestudy

	Light CA glue	Medium CA glue	Epoxy Resin	Polyacrylamide Tackifier
Advantages	Easy application, resistant up to 120 °C	Easy application, resistant up to 120 °C	Strong bond	Liquid application
Disadvantages	Heavy depending on the area, needs moisture to polymerize	Heavy depending on the area, needs moisture to polymerize	Degrades in UV radiation	Must be diluted with water
Cure Time	Seconds	2 Minutes	15 min – 1 hour	N/A
Plastic Type	Thermoplastic	Thermoplastic	Thermoset	Thermoplastic
Cost	\$8	\$10	\$13–\$20	\$30–\$60

	Sodium Polyacrylate	Liquid Acrylic Polymer	PLA Plastic	Acrylic Copolymer
Advantages	Powdered form, easy to pack	Used in concrete, can handle high-shear loads	Lightweight, solid, easy to transport	Liquid application
Disadvantages	Must be mixed with water	Can only be bought by the gallon	Melts, shrinks	Cannot handle high loads
Cure Time	10 seconds	Less than 7 days	15 minutes	None
Plastic Type	Thermoplastic	Thermoplastic	Thermoplastic	Thermoplastic
Cost	\$35	\$35–\$50	\$20	\$9

B. Materials and Methods

In order to test the solutions and their effect on lunar regolith, a JSC-1A lunar regolith simulant was used. It is an engineered material designed to closely replicate the physical and chemical properties of lunar mare soil, specifically the basaltic composition of lunar samples from Apollo missions 14 and 15. Key properties include high lithic and glass content, angular to subrounded particles, and a particle size distribution similar to lunar soil. While it lacks certain lunar features like nanophase iron and agglutinates, it is valuable for geotechnical and ISRU testing. JSC-1A is recommended for studies not critically dependent on iron redox conditions or ilmenite content.

For loose soil samples, the shelly tube is filled with 152 mm of soil carefully placed without compacting. In case of compacted samples, the shelly tube is filled with 3 equal layers (50 mm each) of soil, compacting each layer with 25 blows of 4.5 kg proctor hammer. A filter paper is placed on top, followed by the stopper. Bentonite is then applied to prevent the water leakage down the tube. If a solution is to be applied to the top layer, the piston is raised to make contact with the stopper and is then screwed in clockwise to lock the piston assembly (Fig. 1). The block around the Shelby tube is tightened to ensure the tube is fixed and only the soil raises with the piston.



Fig. 1 EFA block tightening.

To start the experimental procedure, the EFA water tank is filled with water to the fill line. The flow is started at 0.3 m/s, and the initial length of the piston is measured while a 10-minute timer is started. The piston is raised to keep the top of the soil sample flush with the channel. If the piston displacement is more than 10 mm, the process moves on to the next velocity. If the displacement is less than 10 mm, the same velocity is maintained until the 10-minute timer ends. This process is repeated with velocities of 0.4 m/s, 0.5 m/s, 0.8 m/s, and 1 m/s. For treated regolith, these velocities were increased to the maximum flow velocity of 6.5 m/s. To adjust the water flow, the red handle is rotated counterclockwise to increase the flow velocity. At around 1 m/s, the machine piston rate will not be able to keep up with the rate of erosion, at which point the experiment was ended by stopping the flow of water. Some experimental error was introduced due to the motor of the EFA corroding, and an older EFA was used to test the thermoplastic and cyanoacrylate treated lunar regolith. This machine had a tendency to shake violently and was only able to reach a maximum velocity of 4 m/s.

For the application of cyanoacrylate, Bob Smith Industries (BSI) cyanoacrylate glue was chosen due to the high concentration of Ethyl Cyanoacrylate. The super thin and medium viscosities were chosen for testing. A solution of one part cyanoacrylate and 10 parts anhydrous acetone was created for both glue types. 22 mg of each solution was then poured over two Shelby tubes filled with loose regolith simulant. For the PLA plastic solution, first a 0.5 mm circular sheet of PLA thermoplastic was created using a 3d printer. This sheet was then applied to the top of a Shelby tube filled with loose regolith. The sides of the

plastic sheet were glued down using a cyanoacrylate glue. The thermoplastic was not melted, as any attempt to melt the PLA into the regolith caused the plastic to shrink, shrivel, and tear.

Finally a sintering solution was also investigated with the following procedure. A solution of distilled H₂O and unionized salt was created to act as a binder for the lunar regolith simulant. A ratio of 6.25% NaCl by volume was used. A cylindrical mold with a diameter of 40 mm and a height of 25 mm was used to shape the lunar regolith simulant. The mold was created using a 3d printer and was made of PLA. The binder was combined with the regolith at 3.5 parts regolith to 1 part binder. The regolith and binder were then lightly packed into the molds. A total of six samples were created. The samples were then removed from the mold and pre-sintered at 200 C for one hour. They were then removed and placed into a high temperature tube furnace (Fig. 2) with an argon atmosphere to protect the samples from oxidation. Three samples were heated to 1100 C and the other three samples were heated to 1200 C. Both took two hours to get to temperature and were held at their respective temperatures for one hour. The samples were then allowed to cool over a few hours. Once the samples were cooled, they were removed from the argon atmosphere and the tube furnace. The samples were then placed in a 41 mm diameter Shelby tube. The gap between the samples and Shelby tube was again filled with Bentonite to prevent leakage and the samples were tested in the EFA.



Fig. 2 Sintering furnace.

C. Results



Fig. 3 Uncompact regolith.

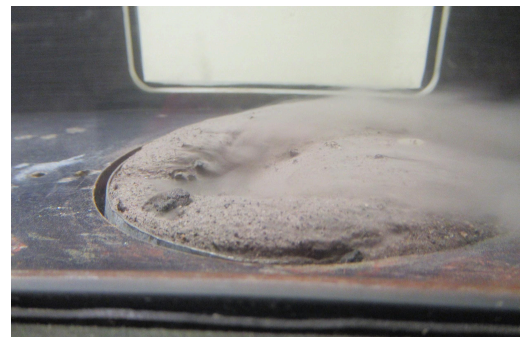


Fig. 4 Compacted regolith.

Both the uncompact and compacted lunar regolith (Fig. 3 and Fig. 4) had high erodibility. The compacted regolith performed marginally better than the uncompact regolith at higher velocities. The uncompact regolith had a density of 1.38 g/cc with a cohesion of 0.361 kPa and the compacted regolith had a density of 1.88 g/cc and a cohesion of 2.035 kPa. The cohesion values were analyzed through a direct shear test (DST) - though this was not the focus of the paper, the values are interesting and should be shared to highlight the differences in these two samples.

The sintered samples (Fig. 5 and Fig. 6) did not appear to have been heated evenly. Thus, 4 out of the 6 samples fragmented while attempting to remove them from the high temperature furnace. The intact sintered regolith did not experience any erosion up to the maximum velocity of 6.5 m/s.

Two thermoplastic-treated samples were also tested. The regolith treated with cyanoacrylate (Fig. 7) did not experience any erosion up to the maximum velocity of 4 m/s, and the regolith treated with PLA thermoplastic (Fig. 8) did not experience any erosion up to the velocity of 4 m/s.



Fig. 5 Lunar regolith sintered at 1100 °C.



Fig. 6 Lunar regolith sintered at 1200 °C.



Fig. 7 Lunar regolith treated with CA.

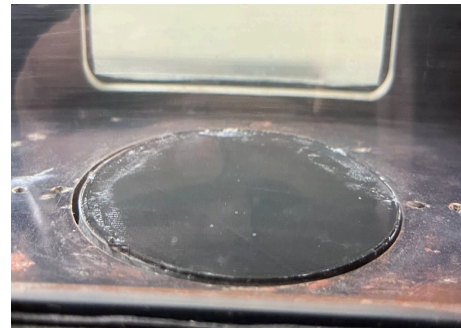


Fig. 8 Lunar regolith treated with PLA.

The erosion curves in terms of velocity and in terms of shear stress (Fig. 9 and Fig. 10) for the above samples are plotted on log scales on top of the erosion categories in Briaud's erosion chart. The results show that the compacted regolith sample has marginally better erosion resistance than the uncompacted trial. The difference in erosion rate between the compacted and uncompacted lunar regolith is likely greater than was measured, as the water soaking into the regolith likely fluidized the regolith, causing its cohesive properties to change. All of the treated regolith samples experienced no erosion. A higher velocity, air based EFA would be needed to do further research on solutions choices.

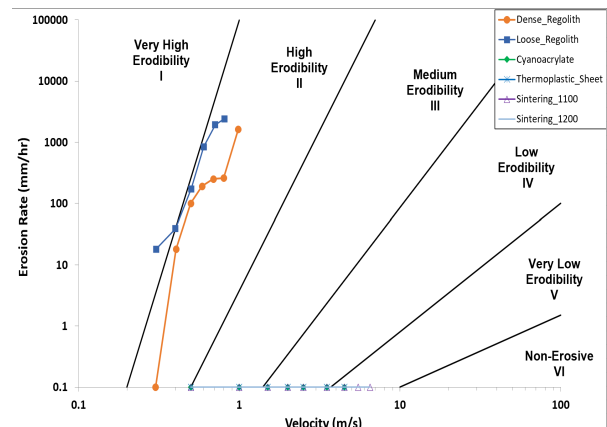
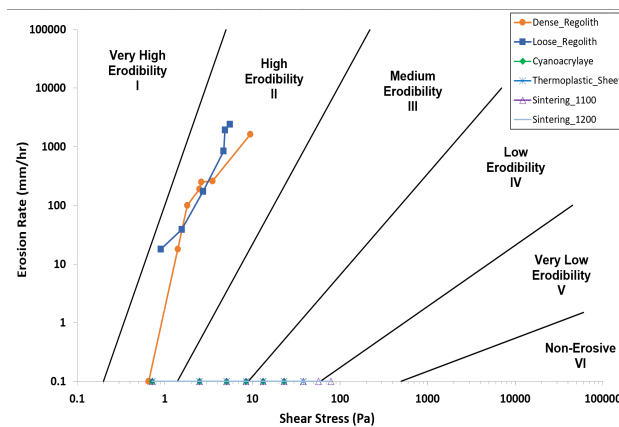


Fig. 9 Erosion rate of different shear stresses. Fig. 10 Erosion rate of different flow velocities.

III. Mathematical Transformation and CFD Analysis

A. Analytical Water-to-Air Transformation

The combined effects of the velocity and dynamic viscosity differences will not allow for a shear stress equivalency to mathematically transform the erosional mechanism in water to that in exhaust gasses. Shear stress in fluids can be described by Newton's Law of Viscosity. However, this formulation reveals that the velocity of the water in the EFA must be about 144 m/s to use the shear stress equivalency for scaling purposes, as shown in the appendix. Since the water in the EFA can only reach a maximum velocity of 6.5 m/s, this shear stress equivalency approach is unrealistic to scale. Therefore, another avenue must be pursued to compare the erosional effects of the two flows. The erosion process is a boundary layer phenomenon, meaning that an analysis of its thickness can be used to formulate a treatment for the comparison of two significantly different fluids. The boundary layer thickness for the laminar and turbulent flow cases is given below, respectively, where x represents the distance along the surface and Re_x is the Reynolds number of the flow given further below in Eq. (3).

$$\delta_L \approx \frac{5.0}{\sqrt{Re_x}}x, \text{ (Blasius solution)} \quad (1)$$

$$\delta_T \approx \frac{0.37}{Re_x^{1/5}}x \quad (2)$$

$$Re_x = \frac{\rho u L}{\mu} \quad (3)$$

By substituting the definition of Reynolds number (Eq. (3)) into Eq. (1) and Eq. (2), these equations can be rearranged into a simple relationship relating the flow properties to the thickness of the boundary layer found in Eq. (4) and Eq. (5) below.

$$\delta_L \approx 5x \left(\frac{\mu}{\rho u L} \right)^{1/2} \quad (4)$$

$$\delta_T \approx 0.37x \left(\frac{\mu}{\rho u L} \right)^{1/5} \quad (5)$$

To compare different flows with these relationships, the ratio between the boundary layer thicknesses of the two flows must be formed as shown below.

$$\text{Laminar Ratio} = \left(\frac{\frac{\mu_w}{\rho_w u_w}}{\frac{\mu_{eg}}{\rho_{eg} u_{eg}}} \right)^{1/2} \quad (6)$$

$$\text{Turbulent Ratio} = \left(\frac{\frac{\mu_w}{\rho_w u_w}}{\frac{\mu_{eg}}{\rho_{eg} u_{eg}}} \right)^{1/5} \quad (7)$$

These boundary layer ratios must be relatively close to 1 for this boundary layer thickness equivalency approach to function. Here, the density of the exhaust gas ρ_{eg} is approximated using the average density of H₂O and CO₂, similar to the process done to find the rough approximation of dynamic viscosity. This density value will also be further refined later in a simulation approach. These boundary layer thickness ratios can be compared for the purpose of later identifying ideal mitigation solutions. Through this method, the presence and profound effects of the slow-moving boundary layer can be properly accounted for to compare the exhaust gas flow on the lunar surface and the EFA water flow.

B. CFD Analysis

The geometries of craters made by plume surface interaction (PSI) with the lunar surface can vary greatly depending on the region of the lunar surface where the landing occurs. Much of contemporary PSI research is based on the Apollo landers which landed near the Moon's equator, and may have produced shallower craters than predicted in the south pole highland environment. Considering that the exact erosion mechanisms and subsequent crater geometries are not fully understood yet, it is not particularly useful to model continuum mesh-morphing to base mitigation decisions. Rather, it is much more useful to consider a set of static crater geometries that cover the basic range of possible lunar regolith properties. The flow properties at the impingement point and tangentially along the surface can be determined and used to draw conclusions about the effectiveness of proposed mitigation solutions. These static crater assumptions are based on the short time interval when the lunar lander is burning closest to the surface, where the erosion begins to have diminishing effects due to the lunar regolith's rapidly increasing relative density with depth.

Three nominal static crater geometries are considered for the varying possible outcomes expected from empirical data taken during the Apollo missions as well as the expected lunar properties at the south pole, where the Artemis site is planned. Crater geometry (a) features a shallow depth and wide radius which is consistent with the lunar crater geometry after the initial 10-cm extremely fine dust layer is eroded away and a hard and dense layer of sediment remains that is much more resistant to further erosion. The Apollo crater was not quite this deep, but it is conservative to assume a greater scour depth of the top fine soil layer due to a larger lander requiring more thrust [2] for landing. Crater geometry (c) assumes a deeper and narrower crater due to a weaker soil that may be found at the lunar south pole highlands, and (b) considers the median case between these two crater geometries.

A direct simulation Monte Carlo (DSMC) method through dsmcFoam+ is utilized for the three static crater geometries due to the varying distance to the lunar surface and the rapid expansion of the pressure field after leaving the exit nozzle not allowing for a continuum flow assumption. This covers the case of particles leaving the crater at high angles, and therefore exiting the continuum flow of the exhaust jet and its deflection, due to considering the flow as it moves into less dense regimes such as transitional flow. The continuum flow condition generally breaks down when the possibilities of rarefied gas effects arise due to the pressure field rapidly diffusing from the exit nozzle. For a vacuum environment of the lunar surface, these rarefied gas effects generally occur when the gas pressure is less than 1000 Pa [3], and the formulation of the exit nozzle conditions is given below. The assumed exit nozzle pressure of 0.01 bar is used due to an exit pressure of 0.1 bar causing inlet particle injection issues, and due to the lack of time left to resolve this considering the computational abilities of this simulation. This simulation therefore will not be the most conservative estimate, although the patterns of pressure and velocity distribution can easily be scaled for the purposes of mitigation solution justification. The derivation of the Knudsen number and associated input properties for the CFD is calculated in the appendix, which determines the exhaust flow at the exit nozzle for the assumed vacuum optimized engine to be a few orders of magnitude within the continuum flow regime [4] as shown below in Fig. 11.

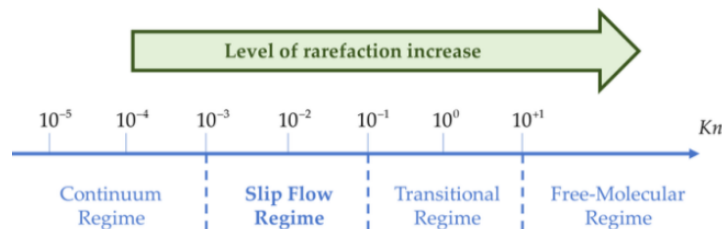


Fig. 11 Flow regimes classified by Knudsen number [3].

From this the flow can be assumed to be in a continuum regime near the jet and its immediate impingement zone, but not beyond this range where the flow can rapidly expand into the vacuum. This continuum assumption will be exploited later for a discrete element method formulation of the surface

effects, but for the particle trajectories the continuum flow regime will not be assumed to account for the diffusing pressure effects on eroded particles. Following these assumed nozzle exit conditions also yields the number density Nd for which the inlet parameter will be defined for the DSMC solver, which is also calculated in the appendix. The subsequent flow analysis results are given below in Fig. 12.

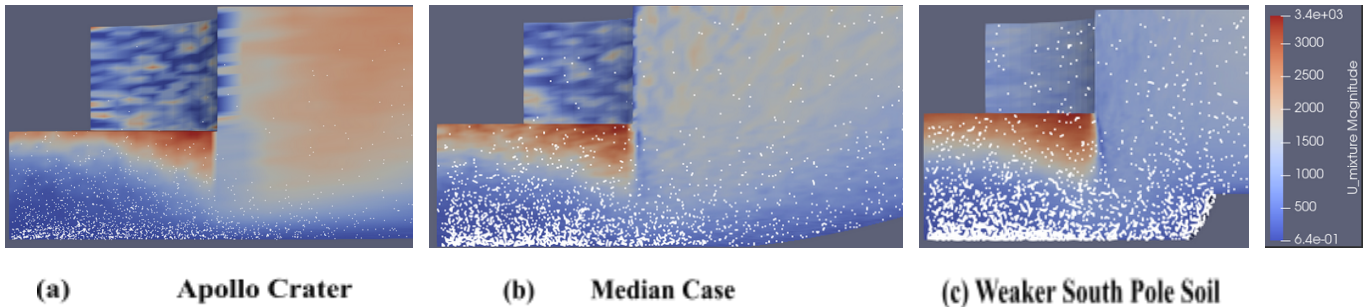


Fig. 12 DSMC flow velocity profile for varying crater geometries.

These flow properties for a vacuum optimized engine 35 cm above the ground match what is expected for an under-expanded exhaust flow expanding before interaction with the lunar surface. Although the mesh and DSMC particle count resolution in this case doesn't have the high fidelity modeling to match that of more computationally powerful investigations, the velocity of the flow can be seen to rapidly attenuate in the short distance to the surface and the pressure similarly rapidly diffuses in the path to the surface as well. Combining these results with the recent literature on PSI justifies the assumption of a slow moving boundary layer [5] tangentially along the surface and a relative (to the surrounding vacuum) high pressure field in the immediate radius on the lunar surface below the nozzle exit. This indicates that the chosen mitigation solution must prevent the pressure diffusion effects that can occur due to the pressure field diffusing into and subsequently erupting from the lunar regolith. The viscous mode of erosion, although certainly a present threat, is driven by the tangential velocity of the impinged flow along the surface and therefore protected by the slow moving boundary layer from any high velocity free stream lines outside this boundary layer.

The literature investigation of particle trajectories also indicates that a deflector based solution alone will not be sufficient since it is unreasonable to assume a high coefficient of restitution for the lunar regolith grains of all sizes. The coefficient of restitution, a measure of elasticity of particle-particle collisions, is not modeled in Fig. 12 due to computational restraints for the given time frame of this investigation but can cause a sand blasting effect [5, 6] that deflects the particles back down based on particle-particle collisions and pressure from the deflected plume. These deflected particles can affect the landing site equipment that was covered horizontally by deflectors. This is not a particularly concerning risk for the initial landing, as there will be no infrastructure set up yet, however a post-landing mitigation solution must account for this by implementing more than just deflectors [6] regardless of deflector geometry.

The effectiveness of varying porosity ϕ can be seen below using a discrete element method (DEM) simulation which assumes a continuum flow from the exhaust nozzle, which is a reasonable approximation when the nozzle is around 2.5 core diameter lengths away from the lunar surface. At this close distance to the lunar surface it is expected that the erosive forces, both through viscous [7] and diffusive erosion mechanisms, will be greatest and therefore best exhibit the effectiveness of lowering the surface porosity through mitigation solutions. To evaluate the effectiveness of mitigation solutions that decrease the surface porosity, the volume fraction of the particles on the top layer of soil is varied. Following this formulation yields the results of varying surface porosity shown below in Fig. 15. This model is a conservative estimate for the expected PSI conditions as the actual flow properties a the

surface will have an attenuated velocity and pressure compared to the exhaust nozzle plane, which will already be vacuum optimized.

The effect of decreasing the effective surface porosity is seen to decrease the number of particles eroded away out of the control volume. This matches what is expected since the boundary layer displacement thickness (BDLT) generally increases as porosity decreases, where the BDLT defines the distance that a free streamline outside the boundary layer is displaced due to the presence of the boundary layer. This BDLT is also more strongly correlated with the effective protection area for soil erosion than the roughness height, although previously this was only found for low velocity cases [9].

The STAR-CCM software which combines computational fluid dynamics (CFD) and Discrete Element Modeling (DEM) was used to model the cohesion behavior. In DEM, the bond between the particles can be simulated by linear cohesion between the particles and parallel bonds. In the former, the bond allows the particles to rotate with respect to each other. While in the latter, the bond does not allow the rotation. The linear cohesion model is used in which the work of cohesion is the parameter that should be defined between the particles to observe the effect of cohesion. Cohesion is connected to the work of cohesion by the following equation.

$$2\pi a = c'\pi R^2, a = R/4 \Rightarrow c' = w/(2R) \quad (8)$$

Here, w is the adhesion between particles in N/m, a is the radius of the surface, which can be considered as a fraction of particle radius R , and c' is the cohesion between the particles. The provided Fig. 15 illustrates the results of four simulations investigating the behavior of particles subjected to a gas flow ejected at 500 m/s from a nozzle. The particles had a mean diameter of 10 mm, and the simulation domain was a cube with length of 600 mm. The simulations were conducted with varying cohesion work of 0, 50, and 100 N/m (0, 50, and 100 kPa, respectively).

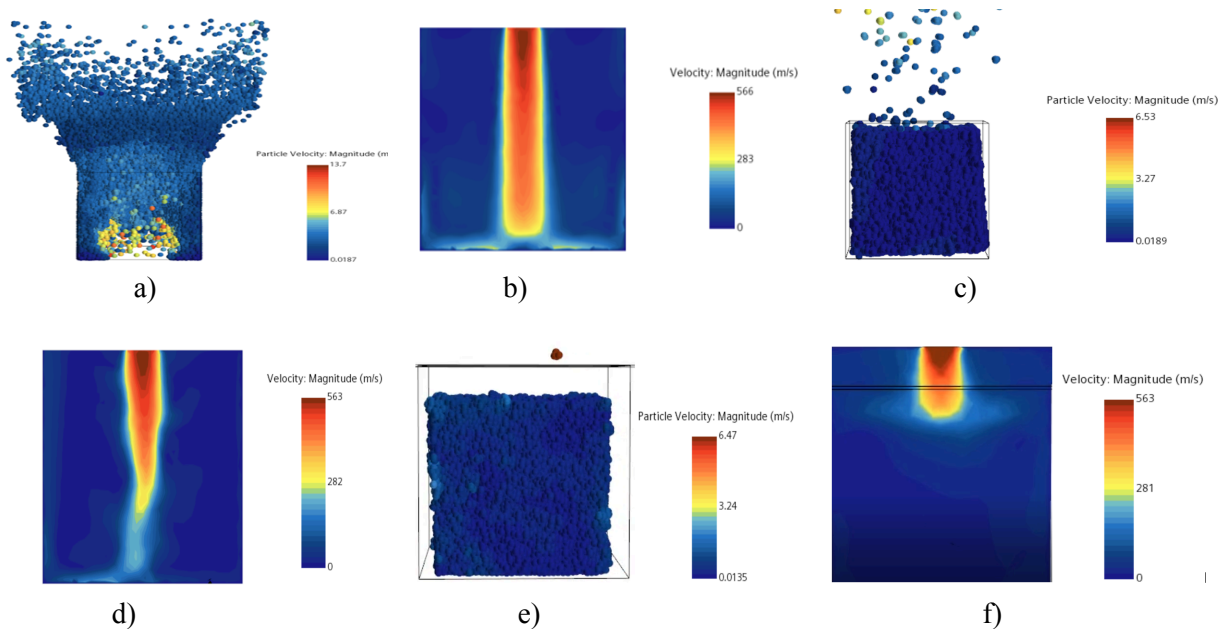


Fig. 13 Particle assembly behavior under high-velocity gas flow with varying cohesion work.

The results demonstrate that with zero cohesion, particles are scattered and dispersed with velocity contours reaching the bottom of the analysis volume, thus forming a deep hole (Fig. 13: a, and b). At 100 kPa cohesion (Fig. 13: e, and f), particles remained intact with no significant hole observed. This underscores the significant influence of cohesion work on the behavior of particle assemblies subjected to high-velocity gas flows. As the work of cohesion increased, the particles exhibited greater cohesion, resisting deformation and dispersion caused by the gas flow.

Table 2 Lunar regolith particle shape properties [8]

Parameter	Average Value	Description
Elongation	1.35	Somewhat elongated
Aspect Ratio	0.55	Slightly-to-medium elongated
Roundness: Silhouette	0.21	Subangular
Roundness: Direct light	0.22	Angular
Volume Coefficient	0.3	Elongated
Specific Surface Area	0.5 m ² /g	Irregular, reentrant

The technique of altering the effective surface porosity is also particularly advantageous due to the angular and irregular nature of the lunar regolith particles as shown above in Table 2 which already provide an effective cohesion from mechanical interlocking of grains. The actual cohesion values [8, p. 507-508] of the lunar regolith are near zero as shown below in Fig. 14, but combining the interlocking grain mechanisms [10] with a solution that fills the void space between grains [11] on the surface as a sort of glue can provide a mass and cost-efficient way to reduce the erosion of lunar soil for subsequent lunar landings.

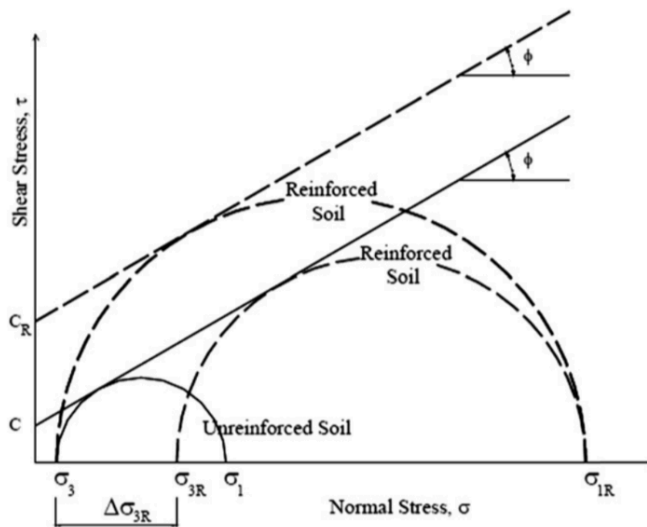


Fig. 14 Apparent cohesion due to mechanical interlocking of grains [10].

This apparent cohesion effect and porosity-lowering mitigation solution will serve to effectively bring the lunar regolith from zone 1 to zone 6 of the erosion category chart as shown below in Fig. 15. This effectively allows the very fine lunar regolith particles to be bound together through mechanical locking from angular particle shapes and through the added binding of a possible polymer or thermoset solution that prevents the exhaust gas diffusing below the surface and causing eruptive erosion as previously found in PSI analyses.

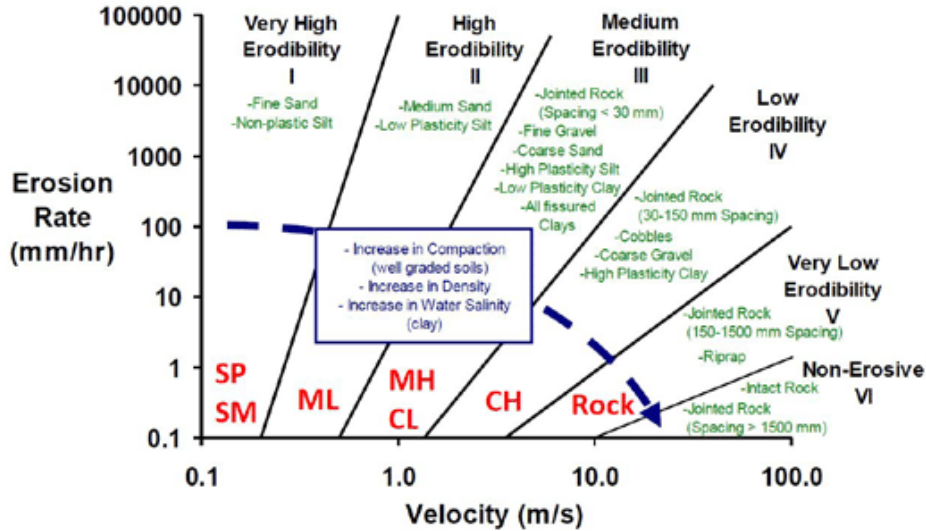


Fig. 15 Erosion categories for varying velocities.

IV. Gas-Granular Erosion Apparatus Design

The EFA served as a starting point for a device that could physically model the plume-surface interaction that is encountered on The Moon. While useful results were still acquired, using water as the testing fluid does a poor job of representing the true interaction between gas and fine granular solid due to the vastly different properties of water and exhaust gasses. The EFA already existed and was available for our use, where useful data could be obtained by comparing different potential solutions to bind the lunar regolith simulant. Still, from the beginning our team knew that in order to gain true insight into PSI something more would be needed. What would grow out of this initial testing is a Gas-Granular Erosion Apparatus (GGEA). This device is similar to the EFA, but instead of using water as a testing fluid, high velocity gas will be used. Lessons learned from the preliminary testing using the EFA have given valuable insight into necessary considerations for a new apparatus. An initial design of the GGEA was developed by our team, and it is likely that more iterations of the apparatus could be developed following testing on an initial prototype, where a clearer image of the ideal device would be gained. The GGEA is a unique device, therefore it is likely that unique issues will arise only after a prototype has been built and used.

The GGEA is a wind-tunnel-type device that tests the erosion rate of a specific prepared or unprepared soil sample exposed to a specific flow in its test chamber. Initially it was thought that two different GGEA types would be required, one for testing subsonic flow and another for testing supersonic flow. Through further analysis and CFD simulations, our team determined that flow along the surface reaches speeds close to 500 m/s, vastly below the nozzle's exhaust velocity of about 3500 m/s. Additionally, flow along the surface in these simulations appeared to be subsonic; there exists a shock wave directly below the nozzle which indicates that the flow downstream of this shockwave is subsonic. Interestingly, even at the high speeds encountered the local properties of the gas allow for the flow at these points to still be subsonic. Therefore, our team came to the conclusion that simply a subsonic version of the GGEA would be sufficient for modeling PSI.

There will be two complimentary configurations of the GGEA for subsonic erosion testing (Fig. 16, 17). In order to more accurately model the desired PSI our team found it would be best to simulate it in two ways. First being the viscous shearing effects of the flow along the surface, and secondly the direct stagnation impingement of flow upon the surface. In order to simulate the shear effects, or viscous erosion, of the flow along the surface a traditional wind-tunnel-type layout is utilized where high-speed subsonic flow passes over a lunar simulant sample which is introduced into the wind tunnel in an identical manner as is seen in the EFA. This allows for one of the erosion mechanisms experienced to be modeled

in a controlled environment. Similar to the testing performed in the EFA, the GGEA will allow for testing lunar simulant samples that are prepared with varying surface preparation methods and materials.

The greatest strength of a device such as this is not necessarily how perfectly the PSI is simulated, but rather in the ability to compare the effectiveness of varying solution methods and materials. It is simple to postulate that one method of preparation of lunar regolith would be superior to another, but our team has actually begun the work demonstrating real physical tests of how these solutions stand up to gas-granular erosion by high speed flow in a controlled environment. Even the EFA, with its limitations as related to its testing in liquid as opposed to gas, allows for the comparison of different potential solutions. This testing will only be improved in the GGEA, by testing in gas our team will eliminate the possibility of water affecting the chemical properties and behavior of our tested solutions.

A rectangular test section of area 0.04 m^2 (200 mm x 200 mm) will be necessary for the purpose of testing erosion along a flat surface, the length of the test section is designed to be 300 mm. The desired flow velocity in the test section is 270 m/s, approximately Mach 0.8. This velocity was chosen in order to avoid compressibility effects encountered above Mach 0.8. A total area ratio of approximately 5:1 was chosen in the design of the GGEA, this led to the maximum area of the tunnel being 450 mm x 450 mm, or 0.2025 m^2 where the flow is at 53.33 m/s. The fan will be located in between the two diffusers, where the area is 0.09 m^2 (300 mm x 300 mm) and the flow at 120 m/s. As for the diffusers that allow for this area ratio, the “principal constraint on the angle is that it be sufficiently small so that the turbulent boundary layer does not separate” [12]. An equivalent cone angle of 3.0 degrees or less was desired for the two diffusers in the GGEA. The only variation between the two configurations in terms of their primary dimensions is that the fan in the GGEA 2.1 is at an area of 0.1225 m^2 (350 mm x 350 mm) where the velocity of the flow will be 88.16 m/s.

Regardless of how well the shear effects are modeled, estimates indicate that viscous erosion mechanism only accounts for less than 10% of total erosion actually encountered in PSI on The Moon. The remaining erosion mechanisms can best be simulated by introducing flow into the testing chamber perpendicular to the surface, similar to how the rocket engine exhaust initially impacts the Moon surface. This alternative configuration of the GGEA will create a stagnation point, which is also encountered below a rocket engine landing on The Moon. The remaining methods of erosion can be tested in this configuration. The layout will go a long way in simulating the diffusion driven flow down through the lunar simulant samples, where we may expect to see an eruption of material. This version of the apparatus varies significantly from the standard configuration of existing wind tunnels; there may be issues encountered that only present themselves once an initial prototype has been constructed and tested.

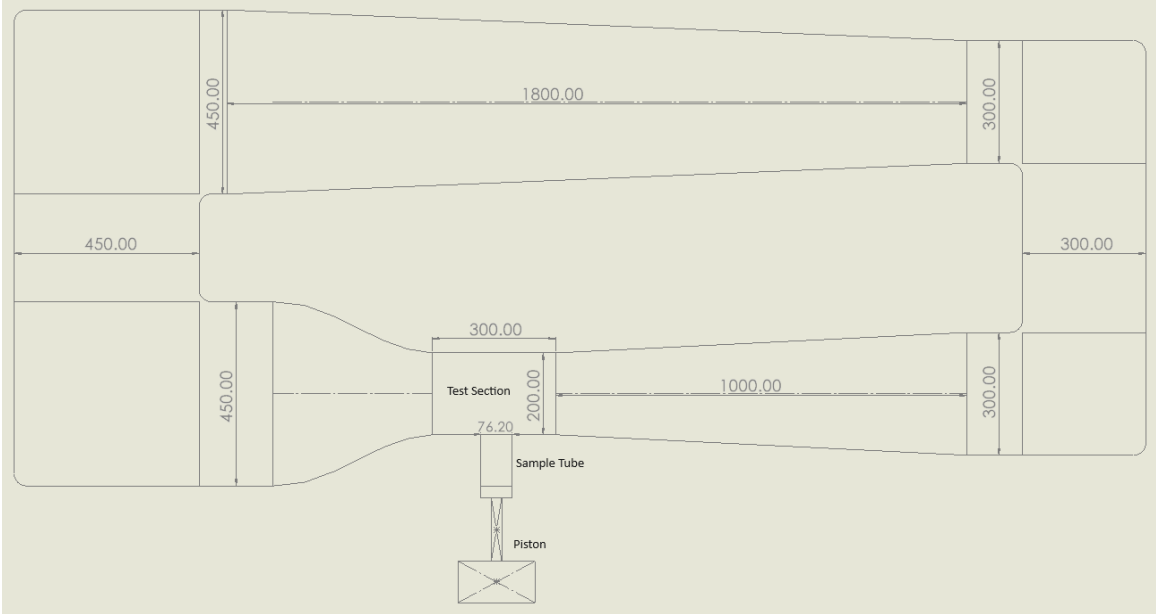


Fig. 16 First iteration of shear erosion testing configuration (GGEA 1.1).

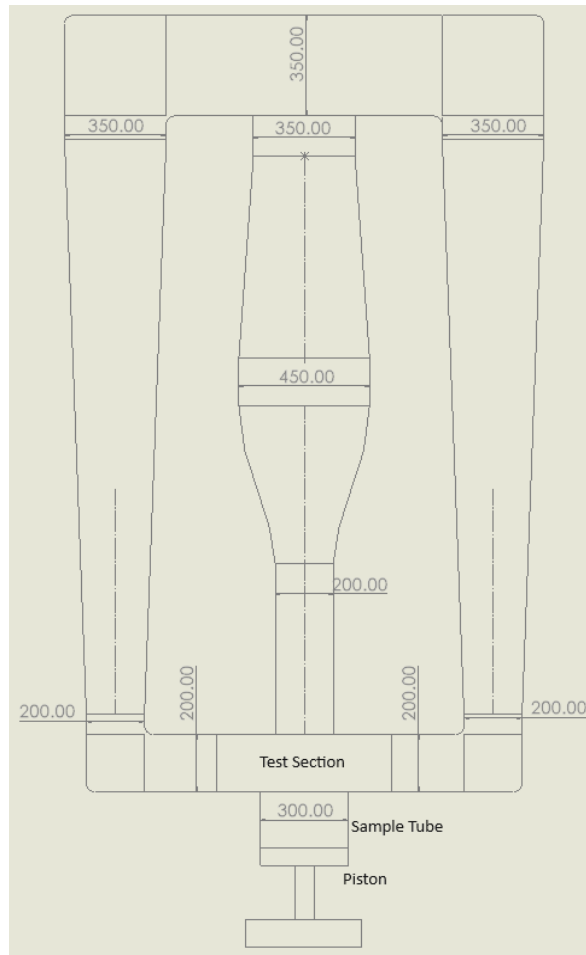


Fig. 17 First iteration of stagnation impingement testing configuration (GGEA 2.1).

Figures 16 and 17 above show the initial concept of the two configurations of the device, GGEA 1.1 and GGEA 2.1 respectively to indicate they are both first iterations. The devices are shown in two dimensions here, both tunnels are square into the third dimension, except for the portion leading into and out of the fan which will be circular. Both regolith sample tubes function in a similar fashion, a piston introduces soil in the tube into the test chamber at a controlled rate, which allows for the rate of erosion to be measured based on the speed of the rising piston. One notable difference between the two configurations is that the sample tube in the second configuration is substantially larger in diameter. The GGEA 1.1 uses the same sized Shelby sample tubes that are used in the EFA. To keep the sample tube the same size in the GGEA 2.1 as those Shelby tubes, the jet of flow above the sample tube would be much larger than the exposed sample, which may affect results. Keeping the apparatus as similar to the PSI seen on The Moon means that the jet of flow should be smaller than the exposed regolith beneath it; thus the sample tube for the GGEA 2.1 has a diameter of 300mm.

The work of estimating the viscous losses throughout the entire GGEA tunnel will be necessary for the determination of the required power of the operating fan motor, P_c , which is the value in the denominator of energy ratio, E_R . Definitions of P_c vary, but the definition chosen here provides a “focus on the aerodynamic aspects of the energy budget and serves to separate clearly the circuit flow properties from the efficiency of the driving fan and the electrical or other driving equipment” [12]. The power required to run the GGEA is a function of the ‘flow losses’ encountered throughout the entire circuit from viscous effects, leaks, etc. In fact, once the tunnel reaches steady-state, the operating motor must have a power equivalent to these circuit losses for operation.

Typical closed circuit wind tunnel actual energy ratios range from 2 to 11. Using the calculated power of flow in the test section (P_t) plugged into Eqn. 16 for energy ratio, along with the typical energy ratio values for existing tunnels one can estimate that the power required to run the GGEA will range from 43,839 W to 241,227 W (approximately 59 hp to 323 hp). Theoretical calculations of the losses in each section of the GGEA were left out due to the already comprehensive nature of this report, and the page limit and time constraints [12].

One point of concern regarding the GGEA was the difficulty of simulating the vacuum conditions encountered on the Moon. In a wind tunnel of this design, it is not feasible to perform this kind of test in vacuum. A pressure-vacuum style wind tunnel could have been used, however this still does not precisely model the PSI on The Moon, where a jet-style source flow is surrounded by vacuum on all sides. The best way to replicate this would be to test in a very large vacuum chamber, with a scaled down engine pointed directly at a bed of lunar simulant. This form of testing would be exceedingly costly and complex. In the basic initial design of the GGEA, testing is performed at atmospheric pressure. It is possible a future iteration of the GGEA will involve reducing the pressure inside of the apparatus, perhaps as near to vacuum as possible.

Another possibility of improving the GGEA in the future would be to implement a cyclonic separator and filter into the circuit. Lunar regolith that becomes entrained in the flow in the GGEA may affect results. Fortunately erosion rate is measured by the rate that the piston introduced additional simulant into the test chamber, and not by dust that is accumulated downstream. Still, having dust still present in the gas that cycles back through the circuit could affect how this now laden gas interacts with the sample in the test chamber. Some thought has been put into ideas for separating the dust particles that are caught in the flow post-erosion. With the extremely fine particle size and the high speeds within the GGEA, there are limited options for removing lunar regolith in the flow. Initially gravity was investigated as an instrument for catching the dust particles, but due to the challenges mentioned above this would not be an effective method.

V. Discussion

A. EFA Assumptions and Errors

In any experiment it is important to find means of error entering the experimentation process and various assumptions made during this process. One major source of error that affected the final results is

the testing apparatus. The original model of the EFA became inoperable during initial stages of testing causing the team to shift to an older model. This model behaves very similar to the original with the exception of the older motor being less efficient causing vibrations. These vibrations cause the soil to move up and down while the Shelby tube is fixed in place. Although the exact quantitative effect of these vibrations cannot be known, the team estimates that these vibrations had the effect of loosening the compaction of the soil therefore causing a loss in erosion resistance.

Another drawback of using an older model of the EFA is that the pump could only accelerate the water to a maximum velocity of 4 m/s flow. Although the treated solutions did not erode, their eroding point could not be analyzed using this machine. Therefore further testing in the GGEA device is needed to verify if the solutions can withstand erosion at higher speeds. This is not the conclusion the team wished to draw, however this does validate the theory that polymer tackifiers can be used to increase the cohesion of lunar regolith and help it withstand erosional forces.

One intentional assumption made during the application of the CA glue on the Shelby tube is that it was allowed to stick to the edges of the tube. This is because on the lunar surface the glue will cover the entire designated surface area and form a plane. The erosion testing in the EFA is testing the middle of the glue layer which can be approximated as an infinite plane. If the glue layer is separated from the tube, it is not appropriately accurate to what the final layer on the lunar surface will be like.

B. Solution Application on Lunar Surface

The erosion testing done will allow for the ideal solution material to be chosen, which maximizes the binding effectiveness while keeping mass cost and energy cost low. So far in the EFA testing, the CA glue has proven to be the most effective solution. However, further testing in the GGEA will either confirm, or alternatively prove that another solution would be most effective.

The method of application for these solution materials will rely upon a smaller robotic mission arriving at the landing site ahead of the crew missions to The Moon. This Commercial Lunar Payload Service (CLPS) lander will deploy an appropriately sized rover which will autonomously apply the solution material to the pre-selected landing site on The Moon. This application method poses no risk to the crew since it is completely autonomous. This application technique will consist of applying the mixed acetone and CA solution on the lunar surface out of a funnel and an external misting device spraying water to add humidity. This mist is necessary for the curing process of the CA to activate.

The cured CA can withstand higher temperatures well with a maximum rated temperature of 220 degrees F however it suffers in colder temperatures with a maximum rated temperature of only -40 degrees F. The reason that this is not an issue is because even if the layer on the surface is frozen, it will still stop the sub surface diffusion phenomena and stop the engine plumes from interacting with the surface. Furthermore the low temperatures will cause the layer to become more brittle but the CA layer is intended to break once the weight of the rocket is applied to it.

This is why there is another process of application explored by our team. While some preparation can be done prior to the first human mission returning to The Moon, a far more effective method of application could be performed by the astronauts themselves when they arrive. Understandably, some level of preparation is desired before any crewed missions arrive. While the autonomous rover can likely perform this basic level of application, a more permanent landing site preparation could be implemented after humans return to The Moon's surface. The Artemis program intends to bring astronauts back to The Moon surface for a much greater duration of time, this time may allow for the astronauts there to perform a more intricate method of application that could not be performed by the previous autonomous rover. Before this rover is sent to prepare the landing site, it will require testing on Earth. Operating the rover and practicing the application of the binder will take place in a vacuum chamber with unprepared lunar regolith simulant inside. Simulating the conditions encountered for the specific landing site chosen for the Moon landing will give the opportunity to prove that the rover will be able to prepare a large section of lunar regolith, for the future planned man landings.

An essential aspect of the verification process of the landing site preparation is vacuum application testing, which is listed in the timeline below. This testing provides an opportunity to verify the resilience

of chosen solution materials when applied to lunar simulant, before they are actually implemented on The Moon. An apparatus could be constructed on Earth similar to existing testing devices where satellite resilience is tested against thermal cycling and high-energy cosmic rays in vacuum. This form of testing would be ideal to verify that whatever solution material is ultimately chosen is able to withstand the extreme temperature fluctuations, and high-energy radiation present on The Moon’s surface. Ideally landing site preparations would be long lasting improvements to the lunar regolith. Certain solution materials will be more susceptible to the consequences of these effects, it will be essential that we test this on Earth before a solution is sent and applied to The Moon’s surface.

VI. Further Implementation

A. Realistic Cost, Schedule and Milestones

This testing and solution methodology is innovative, so analogous scheduling estimates are difficult: the team’s intuition and experience were used to design a schedule with margins of error.

The development period is estimated to be around two years long, in which different sealing and stabilizing methods will be tested in the EFA and construction of the GGEA takes place. In addition, the transformations between air and water will be verified and validated during this stage. The next 2 year period will be operations which includes testing and validation of the EFA solution in the GGEA. As well as a vacuum application testing, preparation of the CLPS lander, and finally launch preparations. At the end of the 4 year period, the solution will be ready to be used on the HLS.

The cost breakdown was acquired from NASA’s Cost Estimation Toolkit (CET), and the budget will grow accordingly over time until the launch of the CLPS lander. 2024: \$981,000, 2025: \$1,009,000, 2026: \$2,373,000, 2027: \$3,095,000. These values take into account the cost of materials, technology maturation, software, system development, production, and labor for management, administrative, technical, and operational services, among other costs.

B. Full Mission Timeline

In correspondence to the mission objectives and milestones stated above, the team devised a timeline that shows the path to adoption.

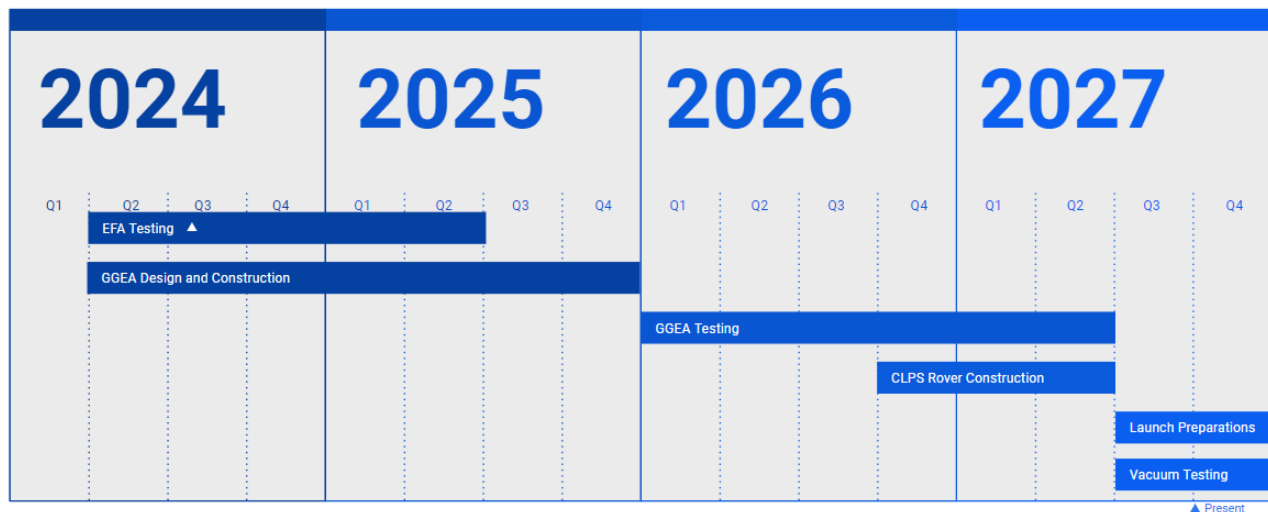


Fig. 18 Full mission year-by-year timeline.

Appendix

A. Nomenclature

c	= cohesion, Pa
du/dy	= shear rate of deformation, s^{-1}
L	= characteristic length, m
u	= velocity, m/s
μ	= dynamic viscosity
σ	= total stress applied normal to the shear plane
τ	= shear force
ϕ	= friction angle
λ	= mean free path, m
Kn	= Knudsen number, dimensionless
ρ	= density, kg/m^3
ν	= kinematic viscosity, m^2/s
δ	= boundary layer thickness, m
Re_x	= Reynolds number, dimensionless
P_t	= Power of flow in test section, W
P_c	= Rate of flow losses in circuit, W
E_R	= Energy Ratio

Superscripts

' = effective

Subscripts

eg	= exhaust gas
w	= water
L	= laminar flow
T	= turbulent flow

B. Intermediate Calculations and Derivations

$$\tau = \mu \frac{du}{dy} \quad (9)$$

Here, the dynamic viscosity of the exhaust gas μ_{eg} can be roughly approximated as the mean value between the dynamic viscosities of the combustion products, CO_2 and H_2O . This rough approximation will be refined further later in this analysis. The velocity difference du is assumed to be the velocity of the fluid subtracted by the velocity at the surface, which is zero, due to the no-slip condition. The distance to the surface dy for both cases of the exhaust gas on the lunar surface and the water testing in the erosion function apparatus (EFA) is assumed to be the same and therefore Eq. (1) can be reduced as shown below.

$$\tau = \mu_w u_w = \mu_{eg} u_{eg} \quad (10)$$

$$\tau = \mu_w u_w = \mu_{eg} u_{eg} \Rightarrow u_w = \frac{0.0000350 \text{ Pa} \cdot s * 3500 \text{ m/s}}{0.00853 \text{ Pa} \cdot s} = 143.61 \text{ m/s} \quad (11)$$

Assuming a methalox based engine at stoichiometric conditions with $T_e = 600 \text{ K}$, $p_e = 0.01 \text{ bar}$, and $u_e = 3500 \text{ m/s}$ assumed at the nozzle exit plane



$$m_{\text{CO}_2} = 1 \text{ mol} \cdot 44 \text{ g/mol} = 44 \text{ g} \quad (13)$$

$$m_{\text{H}_2\text{O}} = 2 \text{ mol} \cdot 18 \text{ g/mol} = 36 \text{ g} \quad (14)$$

Mass fractions of the exhaust gas:

$$\chi_{\text{CO}_2} = \frac{44 \text{ g/mol}}{44 \text{ g/mol} + 36 \text{ g/mol}} = 0.55 \quad (15)$$

$$\chi_{\text{H}_2\text{O}} = \frac{36 \text{ g/mol}}{44 \text{ g/mol} + 36 \text{ g/mol}} = 0.45 \quad (16)$$

Therefore the dynamic viscosity and density of the exhaust gas can be approximated following these mass fractions as

$$\mu_{eg} = \frac{1}{\frac{\chi_{\text{CO}_2}}{\mu_{\text{CO}_2}} + \frac{\chi_{\text{H}_2\text{O}}}{\mu_{\text{H}_2\text{O}}}} = \frac{1}{\frac{.55}{3.74e-5 \text{ Pa}\cdot\text{s}} + \frac{.45}{3.26e-5 \text{ Pa}\cdot\text{s}}} = 3.5076 \times 10^{-5} \text{ Pa}\cdot\text{s} \quad (17)$$

$$\rho_{eg} = \frac{1}{\frac{\chi_{\text{CO}_2}}{\rho_{\text{CO}_2}} + \frac{\chi_{\text{H}_2\text{O}}}{\rho_{\text{H}_2\text{O}}}} = \frac{1}{\frac{.55}{0.00882 \text{ kg/m}^3} + \frac{.45}{0.00361 \text{ kg/m}^3}} = 0.005349 \text{ kg/m}^3 \quad (18)$$

Using these approximated exhaust gas flow properties, the Knudsen number can be calculated for the flow at the nozzle exit which allows the flow regime to be determined.

$$M_{eg} = \chi_{\text{CO}_2} M_{\text{CO}_2} + \chi_{\text{H}_2\text{O}} M_{\text{H}_2\text{O}} = 0.55 \cdot 0.044 \text{ g/mol} + 0.45 \cdot 0.018 \text{ g/mol} = 0.03230 \text{ g/mol} \quad (19)$$

$$m_{eg} = \frac{M_{eg}}{N_A} = \frac{0.03230 \text{ g/mol}}{6.02e23 \text{ molecules/mol}} = 5.3654 \times 10^{-26} \text{ kg/molecule} \quad (20)$$

Assuming a characteristic length of $L = 1$, the Knudsen number is then

$$Kn = \frac{\lambda}{L} = \frac{\mu_{eg}}{\rho_{eg}} \sqrt{\frac{\pi m_{eg}}{2k_B T_{eg}}} = \frac{3.507e-5}{0.005349} \sqrt{\frac{\pi \cdot 5.3654e-26}{2 \cdot 1.380649e-23 \cdot 600}} = 2.09125 \times 10^{-5} \quad (21)$$

Using the above calculated parameters the number density, which is an important input parameter for the CFD, can be calculated.

$$Nd = \frac{N_A \cdot \rho_{eg}}{M_{eg}} = \frac{N_A \cdot \frac{\rho_{eg}}{R T_{eg}}}{M_{eg}} = \frac{6.02 \cdot 10^{23} \text{ molecules/mol} \cdot \frac{10^3}{311.59 \cdot 600} \text{ kg/m}^3}{0.03230 \text{ kg/mol}} = 9.97 \times 10^{22} \text{ molecules/m}^3 \quad (22)$$

Power of flow in the test section of the GGEA

$$P_t = \dot{m}_t (KE)_t = (\rho_t A_t V_t) \left(\frac{1}{2} V_t^2 \right) = 482,233.5 \text{ W} \quad (23)$$

$$E_R = \frac{P_t}{P_c} \quad (24)$$

References

- [1] Briaud, J.-L., *Geotechnical Engineering: Unsaturated and Saturated Soils*, 2nd ed., John Wiley & Sons, 2023.
- [2] Metzger, P.T., “Dust Transport and its Effects Due to Landing Spacecraft,” *Lunar Planetary Institute*, Feb 2020.
- [3] A. Jeerasak Pitakarnnop, R. W., “Rarefied Gas Flow in Pressure and Vacuum Measurements,” *ACTA IMEKO*, June 2014.
- [4] Stéphane Colin, C. B. C. L. B., José M. Fernández, “Review of Optical Thermometry Techniques for Flows at the Microscale towards Their Applicability to Gas Microflows,” *Micromachines*, October 2022.
- [5] Shah Akib Sarwar, Z. H., “Investigating Collision Effects on Lunar Soil Particles Ejected Under Rocket Plumes,” *Acta Astronautica*, 2024.
- [6] A. B. Morris, P. L. V. L. M. T., D. B. Goldstein, “Modeling the Interaction Between a Rocket Plume, Scoured Regolith, and a Plume Deflection Fence,” *Thirteenth ASCE Aerospace Division Conference on Engineering, Science, Construction, and Operations in Challenging Environments, and the 5th NASA/ASCE Workshop on Granular Materials in Space Exploration*, 2012.
- [7] A.B. Morris, P. L. V. L. M. T., D. B. Goldstein, “Plume Impingement on a Dusty Lunar Surface,” 2011.
- [8] W. David Carrier III, G. R. O., and Mendell, W., “Lunar Sourcebook, Ch. 9: Physical Properties of the Lunar Surface,” Tech. rep., Lunar and Planetary Institute, 1991.
- [9] Shuai Zhang, M.-H. Y. G.-I. G. Y.-Y. Z. L. W. Y.-Z. W., Guo-Dong Ding, “Application of Boundary Layer Displacement Thickness in Wind Erosion Protection Evaluation: Case Study of a Salix Psammophila Sand Barrier,” *Int J Environ Res Public Health*, Feb 2019.
- [10] Jonathan T. H. Wu, T. P., “Load-Carrying Capacity and Require Reinforcement Strength of Closely Space Soil-Geosynthetic Composites,” *Journal of Geotechnical and Geoenvironmental Engineering*, September 2013.
- [11] Philip T. Metzger, J. E. L., Jacob Smith, “Phenomenology of Soil Erosion Due to Rocket Exhaust on the Moon and the Mauna Kea Lunar Test Site,” *Journal of Geophysical Research: Planets*, 30 June 2011.
- [12] Barlow, Jewel, et al. *Low-Speed Wind Tunnel Testing*. 3rd ed., John Wiley & Sons, Inc.
- [13] Sohair Al-Khatatbeh, M. A., Maha M. Salloomi, “Effect of Particle Size Distribution on the Sintering Behavior and Properties of Ceramic Tiles,” *Ceramics International*, July 2022.
<https://doi.org/10.1016/j.ceramint.2022.07.329>.
- [14] ARES, NASA, “JSC-1A Lunar Regolith Simulant,” NASA, 2023.
<https://ares.jsc.nasa.gov/projects/simulants/jsc-1-1a.html>.